THE JOURNAL OF PHYSICAL CHEMISTRY B

ARTICLE

pubs.acs.org/JPCB

On the Cause of Controlling Affinity to Small Molecules of Imprinted Polymeric Membranes Prepared by Noncovalent Approach: A Computational and Experimental Investigation

G. De Luca,* L. Donato, S. García Del Blanco, F. Tasselli, and E. Drioli

Research Institute on Membrane Technology (ITM-CNR), University of Calabria, Via P. Bucci, I-87030 Rende (CS), Italy

ABSTRACT: Imprinting technique applied to membrane preparation via phase inversion methods yields membranes with enhanced affinity toward target molecules. In the imprinted membranes prepared by noncovalent approach hydrogen bond and electrostatic interactions can play a crucial role in determining the performance of these membranes. In this work, quantum mechanical calculations and experiments were performed to understand the physical−chemical causes of the affinity increase in imprinted polymeric membranes to 4,4′-methylendianiline (MDA), dissolved in an organic solvent. An ad hoc synthesized copolymer of acrylonitrile and acrylic acid was used to prepare the membranes. The calculated binding energies show that the hydrogen bonds and electrostatic interactions among polymeric chains are comparable to the strength of the same interactions occurring between polymer and MDA. Using this result and correlated experimental data, this work concluded that one of the causes responsible for the increased affinity of the imprinted membranes is the augmented availability of free carboxylic groups in the nanocavities of the membranes. However, along with this reason, the membrane pore sizes must evermore be taken into account. The knowledge acquired in this study helps us to better understand the mechanisms of molecular recognition and hence to optimize the design of new imprinted membranes.

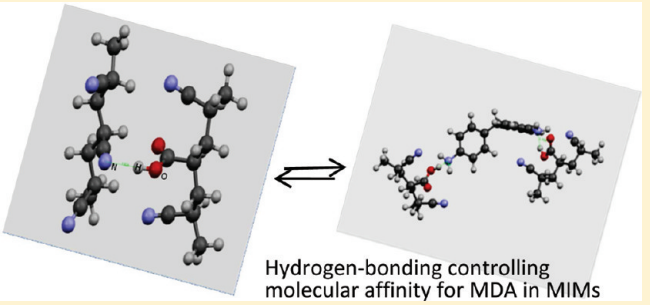

INTRODUCTION

The removal of impurities such as genotoxic substances from different organic solvents applying purification techniques, such as nanofiltration (NF) or molecularly imprinted membranes (MIMs), is a challenge of considerable interest. The combination of different purification techniques is very important because it can contribute to the development of an emerging supradisciplinary field concerning nanostructured polymeric membranes. The knowledge of molecular mechanisms by which NF and MIMs operate is of considerable importance to optimize their design. Hydrogen bonding and weak noncovalent linkages, such as electrostatic interactions and dispersive van der Waals forces, play an important role in many chemical systems. They control the structures of DNA, proteins, molecular recognition, packing and formation of self-assembled aggregates on surfaces. Moreover, the affinity between polymeric membranes and target molecules can be addressed, favoring selective noncovalent intermolecular interactions. Therefore, noncovalent MIMs seem to be promising in the separation of different small molecules.[1,2] Several publications related to MIMs in aqueous media are available.[3−8] On the contrary, works on the removal of small compounds, in particular, genotoxins, from organic solvents are not numerous at all. In this work, the noncovalent MIMs are prepared by casting a polymer solution containing the target molecule; the solvent is partially removed by evaporation, followed by immersion precipitation. Then, the target molecule is extracted with a specific solvent to leave recognition sites in the membrane.[9]

From a theoretical point of view, up to date, there is not a wide literature concerning this topic. However, previous investigations on a similar subject (modified polymeric membranes using additives) have shown that the hydrogen bonding and the short-range electrostatic interactions can often be responsible for marked macroscopic effects.[10,11] Similarly, these noncovalent bonds could also play a crucial role in the molecular recognition that takes place in MIMs. Thus, in this work, a computational and experimental investigation on the cause of the increased affinity of a MIM to the 4,4′-methylendianiline (MDA), dissolved in an organic solvent, was carried out. To achieve this goal, the binding energies between the template molecule and a copolymer of acrylonitrile (AN), functionalized with acrylic acid (AA), P(AN-*co*-AA), were calculated in the frame of density functional theory (DFT). Further to the preparation of MIMs, perm-selective properties and binding tests were carried out to confirm the computational conclusions. Among the different materials used to prepare membranes, polyacrylonitrile (PAN) received much attention because of its thermal stability and resistance to bacterial attack and to most organic solvents.[12,13] Because of these properties, PAN-based MIMs have been prepared by many authors to perform specific separations.[14−17] In addition, Tasselli et al.,[18] studied the influence of different

Received: January 21, 2011
Revised: May 23, 2011
Published: June 28, 2011

functional monomers on the recognition properties of PAN-based MIMs.

MEMBRANE PREPARATION AND CHARACTERIZATION

MDA-imprinted membranes were prepared using the P(AN-*co*-AA) copolymer synthesized by the water-phase precipitation polymerization method.[19,20] A mixture of acrylonitrile and acrylic acid at wt % ratio of 90/10 was copolymerized at 50 °C for 1.5 h under a nitrogen atmosphere and mechanical stirring. The couple $K_2S_2O_8-Na_2S_2O_5$ was used as the initiator system in the presence of Fe^{2+}. Membranes were prepared according to the dry−wet phase inversion method.[21,22] The polymer solution was prepared by dissolving 10 wt % of P(AN-*co*-AA) and 2 wt % of MDA in dimethylformamide (DMF) under stirring at 50 °C until complete homogenization. For comparison, blank membranes were prepared in the absence of the target molecule and used as reference. Polymer solutions were spread onto a glass plate using a casting knife having gap of 400 μm; the solvent (DMF) was partially evaporated at 40 °C for 30 min. Subsequently, the glass plate was immersed in a water coagulation bath. The formed membrane was rinsed with fresh water to remove residual DMF. Acrylonitrile (99%), acrylic acid (99.5%), acetonitrile (ACN, 99%), potassium persulfate, ferrous sulfate, sodium methabisulfite, dimethylformammide (99%), and 4,4′-methylendianiline were purchased from Sigma and used as received.

The prepared membranes were characterized on the basis of their perm-selective properties such as the hydraulic permeance (L_p) and dye rejection.[22] L_p measurements were carried out with pure water in a dead-end filtration cell equipped with a magnetic stirrer, under nitrogen pressure. The membrane surface area (A) was 4×10^{-3} m^2. L_p (l/h·m^2·bar) was determined by measuring the volume of permeate ($V_{permeate}$) collected in a certain time (t) and at pressure (P) of 6 bar according to the following equation

$$L_p = V_{permeate}/(t \cdot A \cdot P) \quad (1)$$

Rejection measurement is one of the most important tests performed to assess the separation properties of membranes. In addition, this test allows us to make an estimation of the membrane pore size based on the molecular size of species that permeate through the membrane.[23] According to this test, solutions of substances with known molecular weight are filtered through the membrane, and the permeate is collected and analyzed. The rejection R (%) is calculated as follows

$$R\ (\%) = 100 \cdot (C_F - C_P)/C_F \quad (2)$$

C_F and C_P are the concentration of the substance in the feed and permeate solution, respectively. It may vary between 0% for substances totally permeable and 100% for substances totally rejected. In this work, the test was carried out by using 10 mg/L solutions of the following dyes: 4-dimethylaminoazobenzene-4′-sulfonic acid sodium salt (methyl orange), 4,4′-(1,1-dioxido-3*H*-2,1-benzoxathiole-3,3-diyl)bis(2-bromo-6-isopropyl-3-methylphenol) (bromothymol blue), and 4,5,6,7-tetrachloro-3′,6′-dihydroxy-2′,4′,5′,7′-tetraiodo-3-oxospiro[isobenzofuran-1,9′-xanthen]-3′,6′ diolate (rose Bengal) in isopropanol (IPA). The experimental setup was the same as that used for the permeability test. The magnetic stirrer provided the agitation of the solution to avoid the build-up of the dye concentration on the membrane surface. The dye concentration was determined via spectrophotometric analysis at wavelengths of 410, 450, and 548 nm for the three aforesaid dyes, respectively. In addition, the prepared membranes were also characterized by IR spectra using a Perkin-Elmer spectrum FT-IR and SEM analysis for morphology observation and thickness measurements.

Binding Tests. Before binding tests were performed, the target molecule was completely extracted from imprinted membranes with ethanol until no MDA was detected in the permeate stream by HPLC measurements. Binding tests were carried out with both imprinted and nonimprinted (blank) membranes in a dead-end filtration cell under magnetic stirring. The cell was connected to a nitrogen cylinder to apply the pressure needed for the filtration test. For each experiment, 200 mL of MDA solution, at 10 mg/L in butanol, was filtered through the membrane under pressure of 6 bar. The filtration time was ∼8 h, during which the total feed solution was filtered through the membrane at permeation flux of 25 mL/h. At the end of each experiment, 200 mL of permeate was collected, making unnecessary any volume adjustment. The measurement of MDA concentration in the feed solution and in the permeate, collected at the end of filtration, allows us to calculate the amount of MDA retained by the membrane by means of the following relationship[18]

$$M_{MDA} = \frac{V(C_F - C_P)}{m} \quad (3)$$

where M_{MDA} is the mass of the retained genotoxin per gram of membrane; C_F and C_P are the MDA concentration in the feed and in the collected permeate solution, respectively; and m is the mass of the membrane. MDA concentrations are determined via HPLC analysis using a LaChrom D7000 HPLC system (Hitachi) equipped with a UV-detector. The column utilized is the Prevail C 18.5 μm 250 × 4.6 mm (Grace). The mobile phase was ACN/water (55/45 v/v), and the flow rate was 1.2 mL/min.

COMPUTATIONAL DETAILS

The quantum mechanical calculations were carried out in the framework of DFT taking into account also the effect of the organic solvent used in the preparation of the membranes. The proposed calculations were performed in the frame of DFT because of its low computational cost compared with post-Hartree−Fock methods. However, it must be kept in mind that using pure quantum mechanic approaches to evaluate the energies of bonds among polymer chains, the choice of chemical models to describe the polymer is crucial. In fact, although DFT methodologies need computational efforts significantly lower than post-HF procedures, large models of polymers cannot currently be used. Consequently, in this work, only the functional groups of polymer with a small part of backbone were taken into account. These structural models inevitably led us to neglect some noncovalent intermolecular interactions or other aspects, even if they may be irrelevant in this work. However, experimental data and tests were used to check the reliability of the polymer models employed here.

The presented results were obtained using the *NWChem* code.[24] Different hybrid functionals have been used to describe hydrogen bonds.[25−29] However, van der Wijst et al.[29] showed that BP86 and PBE functionals also had good recovery ab initio and experimental hydrogen binding energies of DNA base pairs. The calculations of van der Wijst et al.[29] showed that the Becke-Perdew 86 and PBE functionals reproduced the binding energies better than the classical Becke−Lee−Yang−Parr (B3LYP)

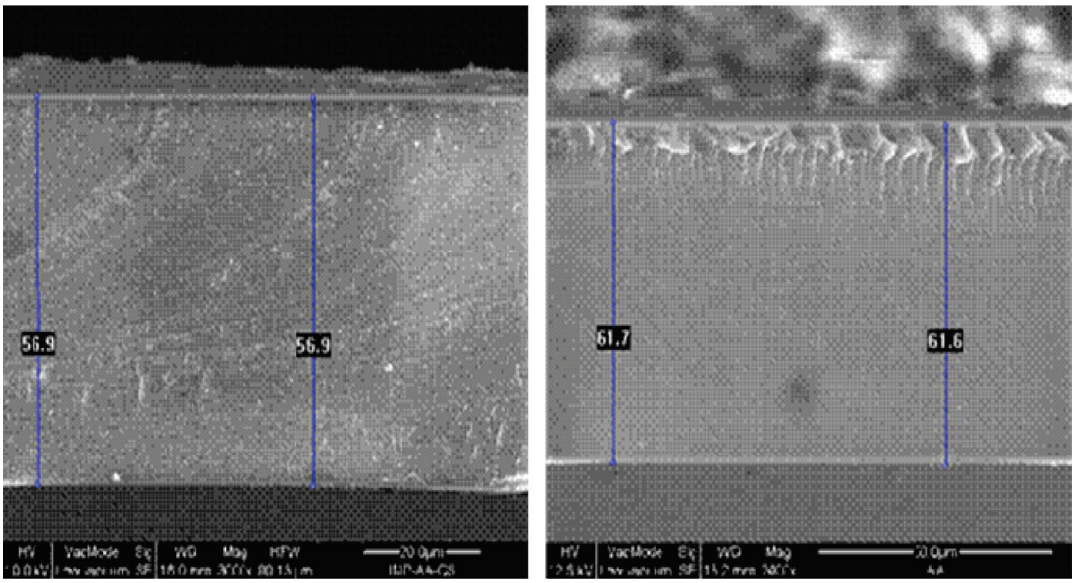

Figure 1. SEM images of the imprinted (left) and nonimprinted (right) membranes cross sections.

functional.[30] The latter functional overestimated these energies by 0.6 (kilocalories per mole) for the adenine−thymine pair and by 0.4 (kilocalories per mole) for the guanine−cytosine However, for the purpose of this work, these errors are acceptable. Moreover, the dispersion energy was evaluated using the empiric long-range contribution of Grimme et al.[31] and then added to the electronic contribution evaluated using B3LYP gave good results.[32] For this reason, the B3LYP potential and energy functional were used in this investigation. The calculations were performed using linear combinations of Gaussian-type orbitals; Coulomb and exchange-correlation potentials were numerically integrated on an adaptive grid with medium accuracy. Triple-ζ orbital basis set with a polarization function (6-311G*) was employed for the atoms of the acid monomers and genotoxine, whereas the 6-31G basis set was used for the remaining monomers of polymer models. The energy convergence threshold was set to 10^{-6} a.u. for the self-consistent field procedure, and the root-mean-square of the electron density was set to 10^{-5} a.u.

All molecular structures were fully optimized using analytical energy gradients with approximate energy Hessian updates. The interaction energies were obtained at the same level of theory used for the optimizations of geometries. The optimization convergence was based on the maximum and root-mean-square gradient thresholds of $(4.5 \text{ and } 3.0) \times 10^{-4}$ a.u., respectively, in conjunction with the maximum and root-mean-square of the Cartesian displacement vectors with thresholds of 10^{-3}. Because the potential electronic surface of the molecular structures considered in this work has many minima with energy lower than KT ($T = 50°$ with K the Boltzmann constant), the Hessian calculations of the optimized geometries were performed on those complexes that are significant for the purpose of the work, as shown below.

The continuum conductor-like screening model proposed by Klamt and Schüürmann[33] was used. In general, continuum models represent a good compromise between accuracy and computational costs. In these models, the cavity, in which the solute is placed, is defined as interlocking atomic spheres constructed using specific atomic radii.[34,35] The radius associated with each atom of solute and the corresponding molecule-shaped cavity are adjustable and are critical parameters in all continuum methods in addition to the response function used to calculate the polarization charges of solvent surrounding the solute.[34,35] Different procedures for the estimation of the atomic radii have been proposed.[35,36] In general, these procedures define these radii to reproduce accurately the experimental solvation free energy of many neutral and charged solutes. Here the default radii implemented in the NWChem package[24] were used. These radii justify the use of an "accessibility solvent" parameter equal to 0.[34] Although these radii could not reproduce with much accuracy most of the aforementioned solvation free energies, in this work, comparisons between binding energies of homogeneous systems were carried out, and thus the accuracy of the absolute values of solvation energies is less important. This issue goes beyond the scope of this Article. Finally, the dielectric constant of the solvent used in the calculations was set equal to 36.7, which corresponds to the dielectric constant of DMF employed in the preparation of the membranes, as underlined in the Membrane Preparation and Characterization section. Moreover, both electrostatic and nonelectrostatic contributions due to the solvent effect were taken into account in the calculation of the binding energies in solvent.

The noncovalent intermolecular interaction energies were evaluated as the difference between the energy of the polymer model−MDA adduct and the energies of the single fragments. The basis set superposition error was therefore included in the calculation of binding energies according to the counterpoise method.[37]

RESULTS AND DISCUSSION

SEM images of the membrane cross sections in Figure 1 show the dense structure of the imprinted and blank membrane. This structure is usually obtained when the slow evaporation of the solvent is allowed. In the same images, the thickness of 57 and 62 μm for the imprinted and blank membrane, respectively, was graphically determined.

Dye rejection data, water, and butanol permeability of the prepared membranes are reported in Table 1. Water permeability

Table 1. Perm-Selective Properties of Prepared Membranes

membrane	L_p (l/m^2·h·bar)		rejection (%)		
	water	butanol	methyl orange	bromotimol blue	rose bengal
imprinted	12	0.8			
blank	14	1	15	40	92

is as low as 12 L/m^2·h·bar, typical of NF membranes. In addition, butanol permeability is lower than water permeability. Because of the similar permeability of the imprinted and blank membranes, dye rejection experiments are performed only with blank membranes. On the basis of rejection results, the prepared membranes are supposed to have a molecular weight cutoff of ~1000 Da.

Results of binding experiments reported in Figure 2 show that the prepared membranes retained a different amount of MDA. In particular, blank membrane exhibits a binding capacity as low as 2.0 μmol/g_{mem}. The imprinted membrane shows a much higher retention, 8.6 μmol/g_{mem}. Therefore, the difference between the imprinted and blank membrane, 6.6 μmol/g_{mem}, gives the specific binding capacity due to the imprinting effect.

In regard to the computational part, the main binding energies are evaluated by building molecular models of the polymer chains. In Figure 3 are reported the molecular-scale models of modified polymer used in the calculations. The bond between the carboxylic hydrogen and carbonyl group (Figure 4a) is the main noncovalent interaction experimented by the P(AN-*co*-AA) polymeric chains in addition to the electrostatic interactions between carboxylic hydrogen and nitrile (Figure 4b). Dispersion interaction among the triple bond of nitriles (Figure 4c) should have lower binding energy with respect to the above interactions. Therefore, the CN−CN bonds were not considered in this analysis. Concerning the main noncovalent interactions among the template molecule and polymer models, they are those between the genotoxin amino group and carboxylic (Figure 5) or nitrile groups. However, as aforementioned, the last interaction should be considered to be lower than the first one. In Tables 2 and 3 are reported the obtained binding energies. These values show that both in solvent and in vacuo the bond energies of polymer−polymer and genotoxin−polymer adducts are comparable. The complexes with the prefix 0 are optimized starting from polymer model geometries having the carbon backbone parallel, whereas the adducts with the prefix 90 are optimized structures starting from geometries with polymer backbone orthogonal. The structure forming a hydrogen bond between carboxylic and nitrile groups is indicated, whereas in the other structures, the hydrogen bonds between two carboxylic groups are not explicitly reported. The orientations of the −CN groups located on the monomers near the acidic functional monomer are important because their orientation determines different steric hindrance with respect to the neighboring carboxylic. In particular, the symbol "i" means that the −CN groups of one polymer fragment are directed inwards of the adduct, whereas the symbol "o" means that the −CN of one fragment are directed outwards of the complex. The $^0(AN_2\text{-}co\text{-}AA)_2^{ii}$ adduct, reported in Figure 6a, shows the lower binding energy both in solvent, −3.4 kcal/mol, and in vacuo, −9.5 kcal/mol. In addition, the binding energies of the more probable adduct, $^0(AN_2\text{-}co\text{-}AA)_2$-$(COOH\cdots CN)^{io}$ reported in Figure 6b, are −4.7 kcal/mol in

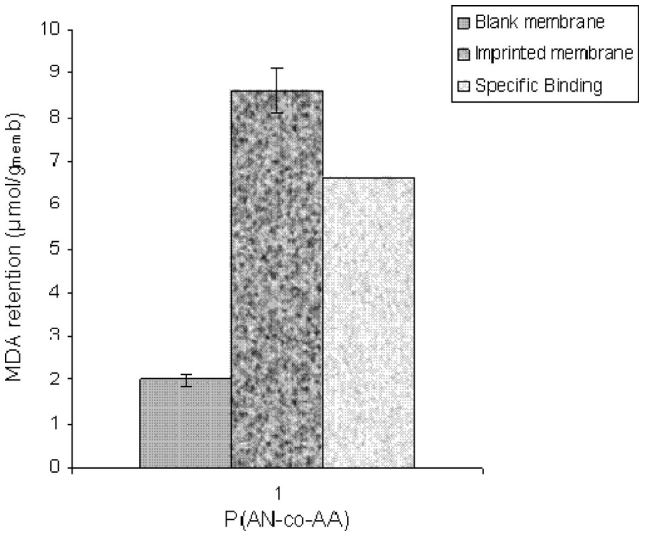

Figure 2. Retained MDA and specific binding capacity of blank and MDA-imprinted membranes.

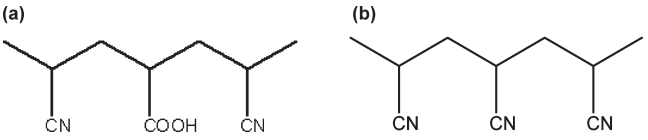

Figure 3. Molecular-scale models (a,b) of modified polymer used in the calculations.

solvent and −13.8 kcal/mol in vacuo. These energies are comparable to the energy of the noncovalent bond involved in the genotoxin−polymer complex shown in Figure 6c. The $^0(AN_2\text{-}co\text{-}AA)_2(COOHCN)^{io}$ adduct would be the more probable with respect because the ratio between the AA and AN monomers, in the copolymer, is equal to 0.1445. The difference between the binding energy of $^0(AN_2\text{-}co\text{-}AA)_2^{ii}$ and $^0(AN_2\text{-}co\text{-}AA)_2^{io}$ complexes is due to the relative orientation of the −CN groups. In fact, these structures form similar hydrogen bonding, but, in the first case, the −CN groups of the fragments are directed inside the complex. This orientation increases the steric hindrance and decreases the correspondent binding energy. Instead, in the $^0(AN_2\text{-}co\text{-}AA)_2^{io}$ structure, the −CN groups of one fragment are directed inside, whereas the ones of the second fragment are directed outside. This orientation decreases the steric hindrance, and at the same time it creates an electrostatic long-range interaction between the −CN groups of one fragment and the hydrogens of the other fragment. The final remark on the values of Table 2 and 3 is related to the highest binding energies. In the case of the polymer−polymer complexes, the highest energies are obtained for the structure shown in Figure 7a $^{90}(AN_2\text{-}co\text{-}AA)_{2c}^{io}$ are −14.3 kcal/mol in solvent and −20.9 kcal/mol in vacuo, whereas for the genotoxin−polymer complexes, the highest binding energy is obtained for the dianiline$\cdots(AN_2\text{-}co\text{-}AA)_2$ (Figure 7b) with energies equal to −14.7 and −25.6 kcal/mol in solvent and in vacuo, respectively. For the $^{90}(AN_2\text{-}co\text{-}AA)_{2c}^{io}$ adduct, the high values of binding energy are due to the formation of a cycle with two hydrogen bonds (Figure 7a), whereas the dianiline$\cdots(AN_2\text{-}co\text{-}AA)_2$ binding energies are caused by the double hydrogen bond formed with two different fragments of the polymeric chains. Although these double interactions are more

dx.doi.org/10.1021/jp2006638 |J. Phys. Chem. B 2011, 115, 9345–9351

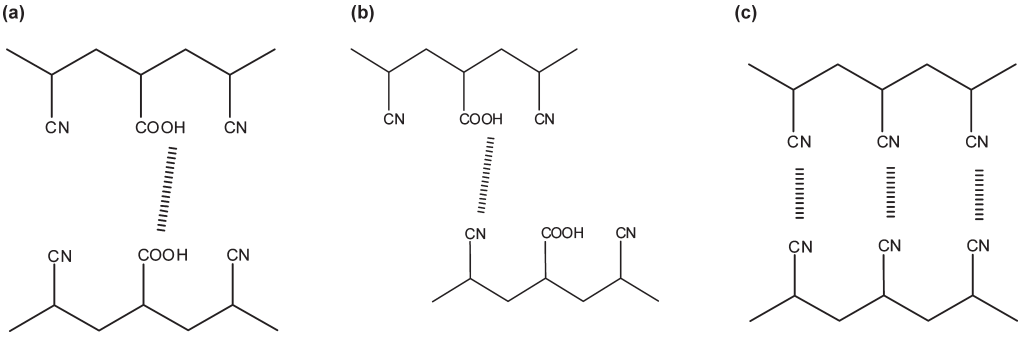

Figure 4. Bond between carboxylic hydrogen and carbonyl group of P(AN-*co*-AA) polymeric chains (a) and the long-range electrostatic interactions between the carboxylic hydrogen and nitrile (b). Dispersion interaction among the triple bond of nitrile groups (c).

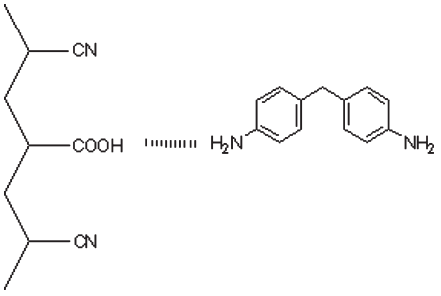

Figure 5. Noncovalent interactions among the genotoxin amino group and the carboxylic group of the polymer.

Table 2. Bond Energies (kilocalories per mole) in DCM Computed at B3LYP/6-311* Level of Theory

complex	ΔE_{BSSE}
$^{0}(AN_2\text{-}co\text{-}AA)_2(COOH^{\cdots}CN)^{io}$	−4.69
$^{0}(AN_2\text{-}co\text{-}AA)_2{}^{io}$	−7.82
$^{0}(AN_2\text{-}co\text{-}AA)_2{}^{oo}$	−3.88
$^{0}(AN_2\text{-}co\text{-}AA)_2{}^{ii}$	−3.40
$^{90}(AN_2\text{-}co\text{-}AA)_{2c}{}^{io}$	−14.25
$^{90}(AN_2\text{-}co\text{-}AA)_2{}^{io}$	−7.50
dianiline$\cdots$$(AN_2\text{-}co\text{-}AA)$	−5.93
dianiline$\cdots$$(AN_2\text{-}co\text{-}AA)_2$	−17.62
$(AN_2\text{-}co\text{-}AA)\cdots$dianiline$\cdots$$(AN_2\text{-}co\text{-}AA)$	−6.00

favored thermodynamically, the probability that these events take place during the formation of the membrane is lower than the probability of single hydrogen bond formation. The two fragments in the dianiline$\cdots$$(AN_2\text{-}co\text{-}AA)_2$ complex may belong to diverse polymer chains or to the same chain. The geometry optimization of the $^{90}(AN_2\text{-}co\text{-}AA)_{2c}{}^{io}$ starts from polymer geometries with orthogonal backbone. After full optimization, this polymer model arranges the carbon backbone in a parallel manner. A comparison between optimized and starting geometries revealed that the rotation of the polymer models from 90 to 0° is due to an arrangement of the polymer backbone in addition to the final rotation of the carboxyl groups. This arrangement can occur because in this study models of the polymer chain were considered. However, using very long chains, this particular arrangement may not occur. In addition, the formation of the cycle can occur when the −CN groups of the polymer model are direct outside the complex. Therefore, although the formation of a cycle with double hydrogen bonding is favored thermodynamically, it should take

Table 3. Bond Energies (kilocalories per mole) in Vacuo Computed at B3LYP/6-311* Level of Theory

complex	ΔE_{BSSE}
$^{0}(AN_2\text{-}co\text{-}AA)_2(COOH^{\cdots}CN)^{io}$	−13.80
$^{0}(AN_2\text{-}co\text{-}AA)_2{}^{io}$	−15.50
$^{0}(AN_2\text{-}co\text{-}AA)_2{}^{oo}$	−12.67
$^{0}(AN_2\text{-}co\text{-}AA)_2{}^{ii}$	−9.49
$^{90}(AN_2\text{-}co\text{-}AA)_{2c}{}^{io}$	−20.91
$^{90}(AN_2\text{-}co\text{-}AA)_2{}^{io}$	−15.44
dianiline$\cdots$$(AN_2\text{-}co\text{-}AA)$	−12.68
dianiline$\cdots$$(AN_2\text{-}co\text{-}AA)_2$	−25.56
$(AN_2\text{-}co\text{-}AA)\cdots$dianiline$\cdots$$(AN_2\text{-}co\text{-}AA)$	−12.70

place after the formation of a single hydrogen bond and then the subsequent rotation of carboxylic groups without the steric hindrance of −CN neighbor groups.

Therefore, the computational results show that the target molecule in the casting solution can effectively bind to the carboxylic functional groups located on the polymer chains. This causes a greater availability of these functional groups once the genotoxin is removed from the casting solution; otherwise, the carboxylic groups would interact by single hydrogen bonds among them (Figure 6a) or with the −CN groups (Figure 6b) giving the more probable structures. The −COOH groups are interacting by hydrogen bond in the blank sample (polymer + solvent). When the target molecules were added to the casting solution (polymer + solvent + MDA), some carboxylic groups will interact with the target molecule because the binding energies of genotoxin−polymer adducts are strong enough to break the bonds between polymer−polymer complexes. Once the template molecules were extracted, these functional groups remain free for successive interactions with basic molecules. The sum of the free carboxylic groups, produced by the random arrangement of the polymeric chains and by the imprinting effect during the membrane preparation, increases the membrane affinity. Therefore, this work concludes that carboxylic groups of the copolymer, interacting via hydrogen bond and long-range electrostatic interactions with MDA, become free and more accessible in the imprinted membranes once the template and solvent are removed.

For verifying this explanation, FT-IR spectra of membranes after target molecule extraction were done. To prepare the samples for the analysis, we dried all membranes in an oven at 90 °C overnight. From the spectra, it was easy to note that the

dx.doi.org/10.1021/jp2006638 |*J. Phys. Chem. B* 2011, 115, 9345–9351

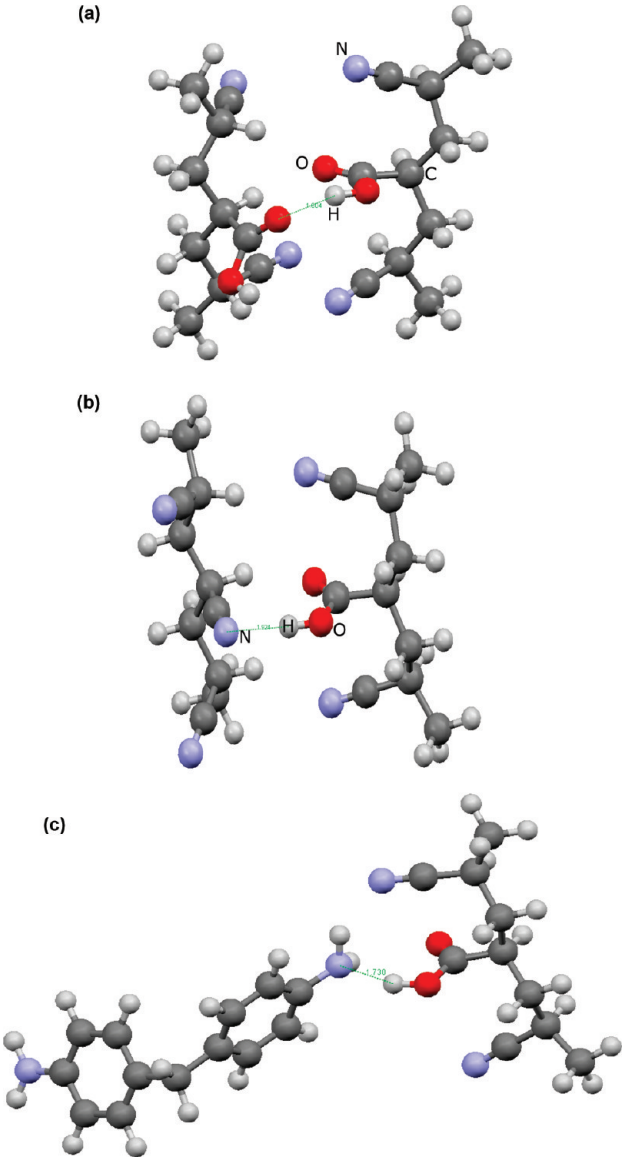

Figure 6. Optimized structure of the $^{0}(AN_2\text{-}co\text{-}AA)_2^{ii}$ adduct (**a**), showing the lower binding energies, of the more probable $^{0}(AN_2\text{-}co\text{-}AA)_2(COOH\cdots CN)^{io}$ adduct (**b**) and the dianiline$\cdots(AN_2\text{-}co\text{-}AA)$ complex (**c**).

amplitudes of the C═O and OH typical stretching bands (C═O: 1653−1795 cm^{-1} = 142 cm^{-1}, OH: 3102−3330 cm^{-1} = 228 cm^{-1}) in imprinted samples were thinner than in the blank samples (C═O: 1641−1814 cm^{-1} = 173 cm^{-1}, OH: 3087−3420 cm^{-1} = 333 cm^{-1}). Larger IR stretching bands mean that more carboxylic groups of the polymer are interacting with each other. The comparison between the area of the C═O and OH peaks cannot be considered because they are not comparable. In fact, the casting solution of blank samples is formed only by polymer and solvent; instead, in the imprinted casting solution, besides polymer and solvent, target molecule is also dissolved. Taking the same quantity of casting solutions, there will be less polymer in the imprinted solution with respect to the blank and, as a consequence, fewer carboxylic groups.

The molecular weight of the target molecule is 198 g/mol, which means that at least five molecules of MDA may enter into

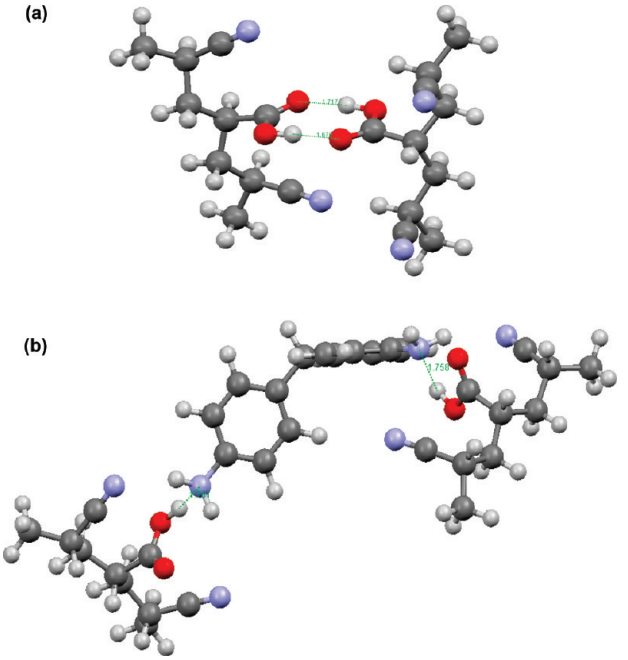

Figure 7. Optimized structure of the $^{90}(AN_2\text{-}co\text{-}AA)_{2c}^{io}$ (a) and dianiline$\cdots(AN_2\text{-}co\text{-}AA)_2$ (b) complexes showing the highest binding energies.

Table 4

molecule	D_{eff} (Å)	D_{RB}/D_{eff}	cross-section ratio
aniline	9.872	1.954	3.817
dianiline	13.980	1.380	1.903
rose Bengal	19.287	1.000	1.000

the membrane pores according to the molecular weight cutoff measurements summarized in Table 1. The correlation between weight and molecular effective size cannot be rigorous and accurate,[38] especially for small molecules. Therefore, the effective diameters of the rose Bengal, dianiline, and aniline were calculated and reported in Table 4. In this Table, the relative cross section ratios were also presented. The effective diameter is defined as the weighed average projection on the membrane surface of the maximum and minimum molecular sizes. The molecular geometries were optimized using the same level of theory described in the Computational Details. The values of Table 4 show that less than two molecules of dianiline can pass through the pores of the membrane, whereas approximately four molecules of aniline can cross the membrane through its pores. Considering the values of Table 4 and the fact that a molecule should have the time to bond with the free and more available carboxylic groups in the pores of the membrane (i.e., to reach the thermodynamic equilibrium), one might predict that the aniline should be retained less than dianiline by both blank and imprinted membranes because the average size of the membrane pores is markedly larger than the size of the aniline molecule; therefore, the effect due to the free carboxylic groups inside the pores should be less pronounced. It is important to emphasize that this aspect is related only to the average size of the membrane pores formed according to the dry−wet phase procedure by which the membranes for NFs are usually prepared.

dx.doi.org/10.1021/jp2006638 |*J. Phys. Chem. B* 2011, 115, 9345–9351

Hence, it is necessary to dissociate the effect caused by the imprinting from that due to the simple size exclusion by the membrane pores. In other words, this second aspect is not directly linked to the imprinting of membranes.

CONCLUSIONS

To understand the cause, at molecular level, determining the increase in affinity of imprinted polymeric membranes, prepared using P(AN-*co*-AA) copolymer and 4,4-methylendianiline as target molecule, we performed a computational and experimental investigation in this work. The attention was focused on this kind of separation because works on this topic are not numerous at all. The increased availability of the carboxylic functional groups, located on the polymer chains, is the driving force for the increased affinity of the membranes to aromatic amine molecules. In particular, the enhancement of the free carboxylic groups in the imprinted membranes is caused by the presence of the basic target molecule in the casting solution during the membrane preparation. Therefore, the sum of free acid groups, produced by the random arrangement of the polymeric chains and those produced by the imprinting effect, increases the affinity of the MIMs. Nevertheless, the average size of the membrane pores must always be kept in mind, although this general factor is intrinsic to the (dry−wet phase) procedure by which membranes for nanofiltration are always prepared.

AUTHOR INFORMATION

Corresponding Author

*E-mail: g.deluca@itm.cnr.it.

ACKNOWLEDGMENT

The research leading to these results has received funding from the European Community's Seventh Framework Programme under grant agreement n° 214226 (New Molecular Purification Technology for Pharmaceutical Production, NEMOPURE). In addition, we are very grateful to CASPUR for the use of High Performance Computers.

REFERENCES

(1) Kobayashi, T.; Takeda, K.; Ohashi, A.; Makoto, M.; Sugiyama, S. *Ther. Apheresis Dial.* **2009**, *13*, 19.
(2) Leea, M. H.; Chin Tsaib, T.; Thomasc, J. L.; Lin, H. Y. *Desalination* **2008**, *234*, 126.
(3) Hillberga, A. L.; Braina, K. R.; Allender, C. J. *J. Mol. Recognit.* **2009**, *22*, 223.
(4) Donato, L.; Figoli, A.; Drioli, E. *J. Pharm. Biomed. Anal.* **2005**, *37*, 1003.
(5) Ku, C.; Faizal, M.; Kobayashi, T. *Polym. Eng. Sci.* **2008**, *48*, 1085.
(6) Silvestri, D.; Barbani, N.; Cristallini, C.; Giusti, P.; Ciardelli, G. *J. Membr. Sci.* **2006**, *282*, 284.
(7) Liu, W.; Wang, B. *J. Appl. Polym. Sci.* **2009**, *113*, 1125.
(8) Fujikawa, S.; Muto, E.; Kunitake, T. *Langmuir* **2009**, *25*, 11563.
(9) Donato, L.; Tasselli, F.; Drioli, E. *Sep. Sci. Technol.* **2010**, *45*, 2273.
(10) De Luca, G.; Gugliuzza, A.; Drioli, E. *J. Phys. Chem. B* **2009**, *113*, 5473.
(11) Gugliuzza, A.; De Luca, G.; Tocci, E.; De Lorenzo, L.; Drioli, E. *J. Phys. Chem B* **2007**, *111*, 8868.
(12) Paul, D.; Kamusewitz, H.; Hicke, H. G.; Buschatz, H. *Acta Polym.* **1992**, *43*, 348.
(13) Zhao, Z. P.; Li, J. D.; Wang, D.; Chen, C. X. *Desalination* **2005**, *184*, 37.
(14) Trotta, F.; Baggiani, C.; Luda, M. P.; Drioli, E.; Massari, T. *J. Membr. Sci.* **2005**, *254*, 13.
(15) Kobayashi, T.; Wang, H. I.; Fuji, N. *Anal. Chim. Acta* **1998**, *365*, 81.
(16) Nie, F. Q.; Xu, Z. K.; Wan, L. S.; Ye, P.; Wu, J. *J. Membr. Sci.* **2004**, *230*, 1.
(17) Noaman, U. H.; Park, J. K. *Polym. Compos.* **2008**, 1006.
(18) Tasselli, F.; Donato, L.; Drioli, E. *J. Membr. Sci.* **2008**, *320*, 167.
(19) Xu, Z. K.; Kou, R. Q.; Liu, Z. M.; Nie, F. Q.; Xu, Y. Y. *Macromolecules* **2003**, *36*, 2441.
(20) Trotta, F.; Drioli, E.; Baggiani, C.; Lacopo, D. *J. Membr. Sci.* **2002**, *201*, 77.
(21) Ramamoorthy, M.; Ulbricht, M. *J. Membr. Sci.* **2003**, *217*, 207.
(22) Mulder, M. *Basic Principles of Membrane Technology*; Kluwer: Dordrecht, The Netherlands, 1991.
(23) Van der Bruggen, B.; Schaep, J.; Wilms, D.; Vandecasteele, C. J. *Membrane Sci.* **1999**, *156*, 29.
(24) Straatsma, T. P.; Apra, E.; Windus, T. L.; Dupuis, M. E.; Bylaska, J.; de Jong, W.; Hirata, S.; Smith, D. M.; Hackler, A. M.; Pollack, T. L.; Harrison, R. J.; Nieplocha, J.; Tipparaju, V.; Krishnan, M.; Brown, E.; Cisneros, G.; Fann, G. I.; Fruchtl, H.; Garza, J.; Hirao, K.; Kendall, R.; Nichols, J. A.; Tsemekhman, K.; Valiev, M.; Wolinski, K.; Anchell, J.; Bernholdt, D.; Borowski, P.; Clark, T.; Clerc, D.; Dachsel, H.; Deegan, M.; Dyall, K.; Elwood, D.; Glendening, E.; Gutowski, M.; Hess, A.; Jaffe, J.; Johnson, B.; Ju, J.; Kobayashi, R.; Kutteh, R.; Lin, Z.; Littlefield, R.; Long, X.; Meng, B.; Nakajima, T.; Niu, S.; Rosing, M.; Sandrone, G.; Stave, M.; Taylor, H.; Thomas, G.; van Lenthe, J.; Wong, A.; Zhang, Z. *NWChem, A Computational Chemistry Package for Parallel Computers*, version 5.1.1; Pacific Northwest National Laboratory: Richland, WA, 2005.
(25) Fonseca Guerra, C.; Bickelhaupt, F. M.; Snijders, J. G.; Baerends, E. J. *J. Am. Chem. Soc.* **2000**, *122*, 4117.
(26) Zhao, Y.; Truhlar, D. G. *J. Phys. Chem. A* **2005**, *109*, 5656.
(27) Leng, Y.; Krstic, P. S.; Wells, J. C.; Cummings, P. T.; Dean, D. J. *J. Chem. Phys.* **2005**, *122*, 244721.
(28) De Luca, G.; Tocci, E.; Drioli, E. *J. Mol. Struct.* **2005**, *739*, 163.
(29) van der Wijst, T.; Fonseca Guerra, C.; Swart, M.; Bickelhaupt, F. M. *Chem. Phys. Lett.* **2006**, *426*, 415.
(30) Becke, A. D. *J. Chem. Phys.* **1993**, *98*, 5648.
(31) Grimme, S. *J. Comput. Chem.* **2006**, *27*, 1787.
(32) De Luca, G. NanoMemCourse EA3 (Nano-Structured Materials and Membranes in the food Industry) Proceedings 2010, A24/L24.
(33) Klamt, A.; Schüürmann, G. *J. Chem. Soc., Perkin Trans.* **1993**, *2*, 799.
(34) Tomasi, J.; Mennucci, B.; Cammi, R. *Chem. Rev.* **2005**, *105*, 2999.
(35) De Luca, G.; Mineva, T.; Russo, N.; Sicilia, E.; Toscano, M. Continuum Dielectric Models for the Solvent and Density Functional Theory: The State of the Art. In *Recent Advances in Density Functional Methods. Part II*; Chong, D. P., Ed.; World Scientific Publishing: Singapore, 1997; Chapter 3.
(36) Barone, V.; Cossi, M.; Tomasi, J. *J. Chem. Phys.* **1997**, *107*, 3210.
(37) Simon, S.; Duran, M.; Dannenberg, J. J. *J. Chem. Phys.* **1996**, *105*, 11024.
(38) Braeken, L.; Ramaekers, R.; Zhang, Y.; Maes, G.; Van der Bruggen, B.; Vandecasteele, C. *J. Membr. Sci* **2005**, *252*, 195.